Journal of Alloys and Compounds 504 (2010) 371–376

Contents lists available at ScienceDirect

Journal of Alloys and Compounds

journal homepage: www.elsevier.com/locate/jallcom

Effect of preparation method on the physical and catalytic property of nanocrystalline Fe_2O_3

Gang Wu[a,b], Xiaoyan Tan[a,c], Guiying Li[a], Changwei Hu[a,*]

[a] Key Laboratory of Green Chemistry and Technology, Ministry of Education, College of Chemistry, Sichuan University, Chengdu, Sichuan 610064, PR China
[b] Department of Basic Courses, Southwest Jiaotong University-E'mei, E'mei, Sichuan 614202, PR China
[c] The Institute of Applied Chemistry, Central South University of Forestry & Technology, Changsha, Hunan 412006, PR China

ARTICLE INFO

Article history:
Received 21 March 2010
Received in revised form 17 May 2010
Accepted 25 May 2010
Available online 4 June 2010

Keywords:
Nanostructured materials
Catalysis
Crystal structure
X-ray diffraction
XPS

ABSTRACT

Nanocrystalline Fe_2O_3 was prepared by five different methods. The samples were characterized by powder X-ray diffraction (XRD), Fourier transform infrared (FT-IR), scanning electron microscopy (SEM) and X-ray photoelectron spectroscopy (XPS). It is found that pure single-phase of α-Fe_2O_3 crystal could be gained via thermal decomposition and ultrasonic-precipitation method, while both α-Fe_2O_3 and γ-Fe_2O_3 are obtained by the other methods. The morphologies and particle sizes of the samples obtained are approximate except that by thermal decomposition. Compared to α-Fe_2O_3, γ-Fe_2O_3 possesses more surface oxygen species "O^-". The activity test indicates that surface oxygen species "O^-" plays a crucial role in the hydroxylation of benzene to phenol with hydrogen peroxide as oxidant.

1. Introduction

In recent years, intensive research efforts have been devoted to the preparation of nanosized crystalline metal oxides because of their unique properties such as large surface areas, abundant surface defects, unusual adsorptive properties and fast diffusivities [1]. The physicochemical property of nanomaterials has close connection with the synthesis technique. Over the years various methods for the preparation of nanoscale material have been developed, including mainly the liquid and solid phase synthesis using inorganic or organic-metallic compounds as precursors [2–5]. The solid-state synthesis procedures are simple and convenient, while liquid phase synthesis is an attractive way often used in the laboratory to prepare high-purity products.

Fe_2O_3 has two typical modifications consisting of hematite (α-Fe_2O_3) and maghemite (γ-Fe_2O_3). The basic structure of γ-Fe_2O_3 is closely related to that of the inverse spinel Fe_3O_4, and α-Fe_2O_3 has a corundum structure. α-Fe_2O_3 and γ-Fe_2O_3 are of considerable importance for scientific and technological applications in heterogeneous catalysis, magnetic recording and integrated microwave devices [6,7]. Recently, it is reported that α-Fe_2O_3 nanoparticles can be applied as catalyst for the removal of carbon monoxide by catalytic oxidation, which has attracted much interest because of its important applications in gas purification, carbon dioxide laser, carbon monoxide gas sensor and pollution control device [8]. The gas sensitivity of α-Fe_2O_3 can be improved remarkably by using the ultrafine α-Fe_2O_3 powders [9]. γ-Fe_2O_3 is widely used as ferrofluids, bioprocessing, magnetic refrigeration, information storage, gas sensor and color imaging [10]. In addition, γ-Fe_2O_3 with large absorbing capacity in a widely frequency range is extensively applied in cryptic aircraft [11]. In such situations, particle size, shape and surface chemistry play crucial roles in controlling properties like saturation magnetization, coercivity, remanent field, blocking temperature and surper-paramagnetism [12–14]. Therefore, much attention has been focused on the selective or exclusive synthesis of iron oxide with a possible crystalline phase for its special application. Synthesis of iron oxide nanoparticles by thermal decomposition of various iron-containing precursors is technologically acceptable, due to the simplicity of the method and high yield. Recently, the relationship between the structure of α-Fe_2O_3 and γ-Fe_2O_3 together with the conditions of the thermolysis of iron-containing precursors has been demonstrated [15].

Phenol is a valuable intermediate for the synthesis of agrochemicals, petrochemicals plastics and medicaments. Currently, the dominating process for the production of phenol is the Huck-process, which involves multi-step synthesis and generates large quantities of by-product acetone [16]. To meet the economic and ecological demands, intensive research efforts have been devoted to the preparation of phenol by direct hydroxylation of benzene in liquid phase. Generally, hydrogen peroxide is selected as oxi-

* Corresponding author.
E-mail address: gchem@scu.edu.cn (C. Hu).

0925-8388/$ – see front matter © 2010 Published by Elsevier B.V.
doi:10.1016/j.jallcom.2010.05.119

dant due to its environmentally friendly features. The catalysts used are mostly transition metal supported on zeolites and other porous materials, such as TS-1 [17], Cu-MCM-41 [18], V-MCM-41 [19], Ti-MCM-41 [20] and Cu-Al_2O_3 [21]. However, their wide industrial applications are limited by the high cost, multi-step preparation as well as relatively low catalytic activity. Hence, many researchers have studied the oxidation reaction with Fe species due to its low cost [22–25]. Among these reported iron-containing catalysts, Fe_2O_3 usually acts as the main catalytic active component in the hydroxylation of benzene to phenol. However, their benzene conversion and especially their phenol yield are relatively poor. Zhang et al. [23] studied the performance of bulk Fe_2O_3 catalyst with the highest benzene conversion of 4.5%.

To investigate the structural dependence of Fe_2O_3 on the preparation method as well as the correlation of catalytic activity with the structure of Fe_2O_3, Fe_2O_3 was prepared by different methods in the present paper. The catalytic performance of Fe_2O_3 in the hydroxylation of benzene to phenol with H_2O_2 as oxidant had also been studied.

2. Experimental

2.1. Preparation

All of the chemicals used in the experiments were analytical grade reagents. Fe_2O_3 nanoparticles used in this study were prepared by the following techniques:

2.1.1. Ultrasonic-precipitation method (Fe_2O_3-UP)

$Fe(NO_3)_3{\cdot}9H_2O$ (4.04 g) and NaOH (1.2 g) were dissolved in 100 mL deionized water at room temperature, respectively. Then sodium hydroxide solution was added dropwisely to iron nitrate solution with vigorous stirring under the vibration of ultrasonic irradiation. After the addition of NaOH, the reaction mixture was constantly stirred under the vibration of ultrasonic irradiation for another 1 h. The precipitate was filtered out and washed with deionized water until pH 7. Then it was dried at 120 °C for 12 h in air and then calcined at 380 °C for 4 h.

2.1.2. Sol–gel method (Fe_2O_3-SG)

4.04 g of $Fe(NO_3)_3{\cdot}9H_2O$ and 4.2 g of citric acid were dissolved completely in 100 mL deionized water, respectively. The iron nitrate solution was added to the citric acid solution. The resulting transparent brown colour solution was evaporated at 90 °C under constant stirring condition and continuous evaporation led to the gel formation. The obtained black colour gel was dried at 120 °C for 12 h in air and then calcined at 380 °C for 4 h.

2.1.3. Micro-emulsion method (Fe_2O_3-ME)

An aqueous solution (20 mL) containing 0.8 g of $Fe(NO_3)_3{\cdot}9H_2O$ was prepared. A reverse micro-emulsion was prepared by mixing this aqueous solution (20 mL) of $Fe(NO_3)_3$ with 5.5 g surfactant (DBS), 25 mL of toluene and n-butanol with the volume ratio of 1:4 under stirring. Aqueous sodium hydroxide (60 mL, 4.0 mol/L) solution was added dropwisely into this emulsion with stirring. After the mixed fluid was stirred for 12 h at room temperature, the obtained suspension was separated with tap funnel and the organic solvent was removed by rotary evaporation. The remaining solid was washed with ethanol and distilled water for several times, respectively. Finally, the solid was dried at 120 °C for 12 h in air and then calcined at 380 °C for 4 h.

2.1.4. Solid-state milling method (Fe_2O_3-SS)

23.5 g of $(NH_4)_2Fe(SO_4)_2{\cdot}6H_2O$ and 7.2 g of NaOH were mixed in the mortar and ground for 1 h at ambient temperature until strong sour was released. The mixture was washed with deionized water until pH 7. The solid precursor was dried at 120 °C for 12 h in air and then calcined at 380 °C for 4 h.

2.1.5. Microwave solid-state method (Fe_2O_3-MS)

The preparation procedure was the same as that of solid-state milling method except the calcination process was replaced by microwave irradiation for about 30 min at middle frequency.

For comparison, large size Fe_2O_3 (denoted by Fe_2O_3-L) was prepared by decomposition of ferric nitrate ($Fe(NO_3)_3{\cdot}9H_2O$) at 380 °C for 4 h.

2.2. Characterization

X-ray powder diffraction (XRD) patterns of samples were obtained on a DX-1000 diffraction instrument with Cu Kα radiation at a wavelength of 0.154 nm. The data were collected over the 2θ range of 10–70° with the step size of 0.02°.

Infrared (IR) spectra of samples were recorded on the Bruker Equinox FT-IR spectrophotometer in the range of 4000–400 cm^{-1} by the KBr pellet method.

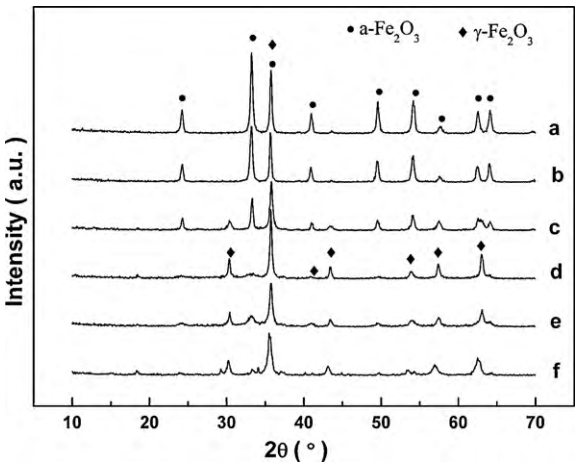

Fig. 1. XRD pattern of Fe_2O_3 prepared by different methods: (a) Fe_2O_3-L; (b) Fe_2O_3-UP; (c) Fe_2O_3-SG; (d) Fe_2O_3-ME; (e) Fe_2O_3-SS; (f) Fe_2O_3-MS.

SEM images of samples were recorded on a FEI/PHILIPS inspect F microscope, at an acceleration voltage of 10 kV and 10.4 mm working distance. Samples were coated with gold before the measurement.

X-ray photoelectron spectroscopies (XPS) of the samples were collected in a Kratos-XSAM 800 Multifunctional Electron Spectrometer using monochromatic Al Kα radiation. The spectrometer was equipped with a DS300 unit for data acquisition. And the binding energies were referenced to the C 1s peak at 284.5 eV. The software XPS Peak Processing was used to deconvolute the peaks to separate different species of the same element.

2.3. Catalytic performance

The direct oxidation of benzene using the above samples was carried out in a three-necked 50 mL round bottom flask equipped with a reflux condenser and a magnetic stirrer. In a typical procedure, 0.4 g of catalyst and 2 mL of benzene (22.56 mmol) were added to 15 mL of glacial acetic acid solvent, and 6 mL (58.2 mmol) of H_2O_2 (30%) was added dropwisely within 10 min under stirring (600 rpm). After all H_2O_2 was added, the reaction mixture was stirred for another 3 h at 343 K. Then, the resulting solutions were analyzed by HPLC (Waters-1525P). An internal standard material, *o*-cresol, was used to quantify the phenol formed. The yield of phenol was calculated as mmol phenol/mmol initial benzene. The selectivity of phenol was calculated as mmol phenol/(mmol phenol + mmol BQ).

3. Results and discussion

3.1. Structural characterization

The X-ray diffraction pattern of the as-prepared samples is illustrated in Fig. 1. For the Fe_2O_3-L and Fe_2O_3-UP samples, the pattern shows (0 1 2), (1 0 4), (1 1 0), (1 1 3), (0 2 4), (1 1 6), (1 1 2), (2 1 4) and (3 0 0) diffraction peaks of α-Fe_2O_3 phase. While for the other samples, the characterized diffraction peaks of γ-Fe_2O_3 are observed at (1 1 1), (2 2 0), (3 1 1), (4 0 0), (4 2 2), (5 1 1) and (4 4 0), in addition to diffraction peaks of α-Fe_2O_3.

It demonstrates that pure single-phase of α-Fe_2O_3 crystal could be gained via thermal decomposition and ultrasonic precipitation method. Both α-Fe_2O_3 and γ-Fe_2O_3 are obtained by SG, ME, SS and MS methods. Weak diffraction peaks assigned to γ-Fe_2O_3 is observed in the Fe_2O_3-SG sample. The content of α-Fe_2O_3 and γ-Fe_2O_3 is almost equal for the Fe_2O_3-ME sample. γ-Fe_2O_3 is the major crystal phase for the Fe_2O_3-SS and Fe_2O_3-MS samples. It suggests that the preparation method significantly influences the formation and distribution of α-Fe_2O_3 and γ-Fe_2O_3 crystal phase. The microwave solid-state method is more favorable for the formation of cubic γ-Fe_2O_3 phase.

The crystallite size was determined using the Scherrer equation:

$$D_{hkl} = \frac{0.89\,\lambda}{\beta \cos\theta}$$

Table 1
Particle size and crystalline phase of Fe_2O_3 prepared by different methods.

Method	Crystalline phase	Particle size (nm)	α-Fe_2O_3:γ-Fe_2O_3
L	α-Fe_2O_3	~350	100
UP	α-Fe_2O_3	25.1	100
SG	α-Fe_2O_3, γ-Fe_2O_3	23.8	80:20
ME	α-Fe_2O_3, γ-Fe_2O_3	23.6	51:49
SS	α-Fe_2O_3, γ-Fe_2O_3	26.0	35:65
MS	α-Fe_2O_3, γ-Fe_2O_3	22.7	26:74

where D_{hkl}, λ, β and θ were the volume-averaged particle diameter, X-ray wavelength, full width at half maximum (FWHM), and diffraction angle, respectively.

The size of α-Fe_2O_3 obtained from the thermal decomposition method is as large as about 350 nm. But the diameters of Fe_2O_3 particles prepared by other techniques are in the nano region and below 100 nm. Since the diffraction peaks of α-Fe_2O_3 and γ-Fe_2O_3 are different, it is possible to distinguish these two phases and calculate the percentage of these two phases. The results are summarized in Table 1. The results demonstrate that the types and fractions of iron oxide are dependent on the preparation method.

Different preparation methods can gain the mixture of α and γ crystal phase of Fe_2O_3 with different relative ratio. It is known that solid-state phase transformation typically proceeds via nucleation and growth. In the present investigation, the interface between two contacting γ-Fe_2O_3 particles can provide the sites for nucleation and the formation of α-Fe_2O_3 phase. Thus, the nucleation rate of α-Fe_2O_3 is determined by the probability of the contact of two γ-Fe_2O_3 particles. For the UP and SG methods, adequate mixing and reaction of raw materials increases the contact of the γ-Fe_2O_3 particles, which act as nucleation sites for the $\gamma \rightarrow \alpha$-$Fe_2O_3$ phase transformation and result in the formation of more smaller α-Fe_2O_3 particles. For the micro-emulsion method, the surfactant-covered water pools offer a unique microenvironment for the formation of nanoparticles. They act not only as microreactors for processing reactions but also exhibit the process aggregation of particles because the surfactants could adsorb on the particle surface when the particle size approaches to that of the water pool. As a result, the particles obtained in such a medium are generally extremely fine and monodispersed [20]. For the SS and MS methods, the nucleation rate of the $\gamma \rightarrow \alpha$-$Fe_2O_3$ phase transformation is much more slower than the growth rate of γ-Fe_2O_3 phase because solid-state preparation method makes against the mixing and reaction of raw materials, thus forming the particles with more γ-Fe_2O_3 and serious agglomeration finally.

3.2. FT-IR spectra

FT-IR spectra for the calcined samples are presented in Fig. 2. The broad band at 3440 cm^{-1} is assigned to the stretching vibration of H_2O, indicating the existence of water absorbed on the samples. Two absorption bands below 1000 cm^{-1} are seen in the spectra, which represent characteristic features of Fe_2O_3 and are assigned to metal oxygen stretching frequencies. Interpretation of the characteristic IR bands has been proposed by Waldron and White [26,27]. The high frequency band γ_1 (~560 cm^{-1}) refers to Fe-O deformation in the octahedral and tetrahedral sites while the low frequency band γ_2 (~480 cm^{-1}) is attributed to Fe-O deformation in the octahedral site. For the Fe_2O_3-L and Fe_2O_3-UP samples, two absorption bands located at 560 and 480 cm^{-1}, which are ascribed to the characteristic absorption bands for pseudocubic shaped α-Fe_2O_3 [21]. The intensity of absorption band at 560 cm^{-1} is stronger than that at 480 cm^{-1}. It gives further evidence for the formation of α-Fe_2O_3 prepared by thermal decomposition and ultrasonic precipitation method. For the other Fe_2O_3 samples, the characteristic IR spectra

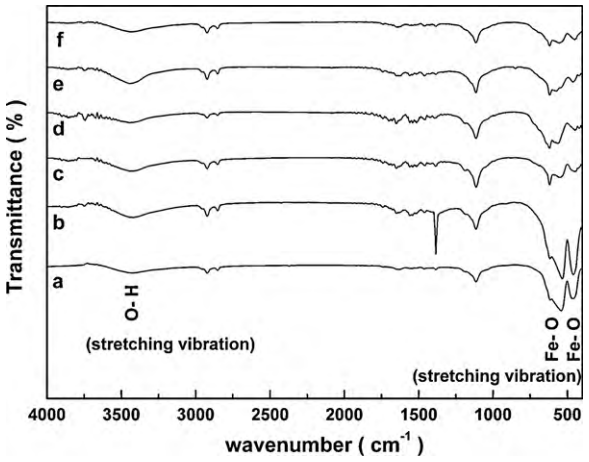

Fig. 2. FT-IR spectra of Fe_2O_3 prepared by different methods: (a) Fe_2O_3-L; (b) Fe_2O_3-UP; (c) Fe_2O_3-SG; (d) Fe_2O_3-ME; (e) Fe_2O_3-SS; (f) Fe_2O_3-MS.

of γ-Fe_2O_3 particles appear at 630, 565 and 460 cm^{-1} [28,29]. In comparison to the Fe_2O_3-L and Fe_2O_3-UP samples, the intensity of absorption band at 560 cm^{-1} decreases greatly. Less amount of α-Fe_2O_3 phase is formed by the SG, ME, SS and MS methods, which is consistent with the XRD result. It also reveals that both α-Fe_2O_3 and γ-Fe_2O_3 co-exist via the SG, ME, SS and MS methods. The observed changes in the intensity of characteristic absorption may be related to the relative ratio of γ-Fe_2O_3 and α-Fe_2O_3 (Fig. 2).

3.3. Microstructure analysis for the particles

The morphologies of Fe_2O_3 particles prepared by different methods are illustrated in Fig. 3. Fe_2O_3 prepared by thermal decomposition is not uniform and the shape varies from round to irregular. While the morphologies of Fe_2O_3 particles prepared by the other methods are almost spherically regular in shape and dispersed uniformly, and these particles agglomerates to some extent due to the interaction between magnetic nanoparticles. It confirms that the preparation method has no obvious influence on the morphologies of Fe_2O_3, except that by thermal decomposition.

3.4. X-ray photoelectron spectroscopy

Due to the approximate crystal structure and lattice parameter of Fe_3O_4 and γ-Fe_2O_3, they cannot be distinguished from each other only by XRD. In order to further confirm the surface chemical states of the samples, XPS technique was performed. Fig. 4A depicts the Fe 2p spectra of the different samples. All Fe 2p spectra reveal the typical structure for iron oxides with broad main peaks (Fe $2p_{3/2}$ and Fe $2p_{1/2}$) and shake-up satellite peaks. The shake-up satellite line is characteristic of Fe^{3+} in Fe_2O_3 [30]. The Fe 2p spectrum for Fe_3O_4 shows broad peaks and no satellite peak due to the overlapping of satellite peaks for Fe^{3+} (at 8.0 eV) and Fe^{2+} (at 6.0 eV) [31]. Furthermore, the δE = B.E.Fe($2p_{1/2}$) − B.E.Fe($2p_{3/2}$) for Fe_2O_3 is found to be higher than that reported for Fe_3O_4 (13.21 eV) [32]. All these observations clearly indicate the absence of Fe_3O_4 in the materials.

Noted that the Fe 2p spectra of α-Fe_2O_3 and γ-Fe_2O_3 are almost identical with each other. In both cases, the main peaks maximum of $2p_{3/2}$ and $2p_{1/2}$ have the shake-up structures at their higher binding energy side at about 8.0 eV. In the present case, this value is found to be ~8.0 eV, which confirms the formation of Fe^{3+}-oxide. However, the marked difference in these XPS spectra is that the binding energy of the main peak, $2p_{3/2}$ is slightly higher in the case of α-Fe_2O_3 (711.3 eV) compared to γ-Fe_2O_3 (710.7 eV). The binding energies of Fe 2p are summarized in Table 2. For the Fe_2O_3-L and Fe_2O_3-UP, the value of Fe $2p_{3/2}$ obtained here matches very well

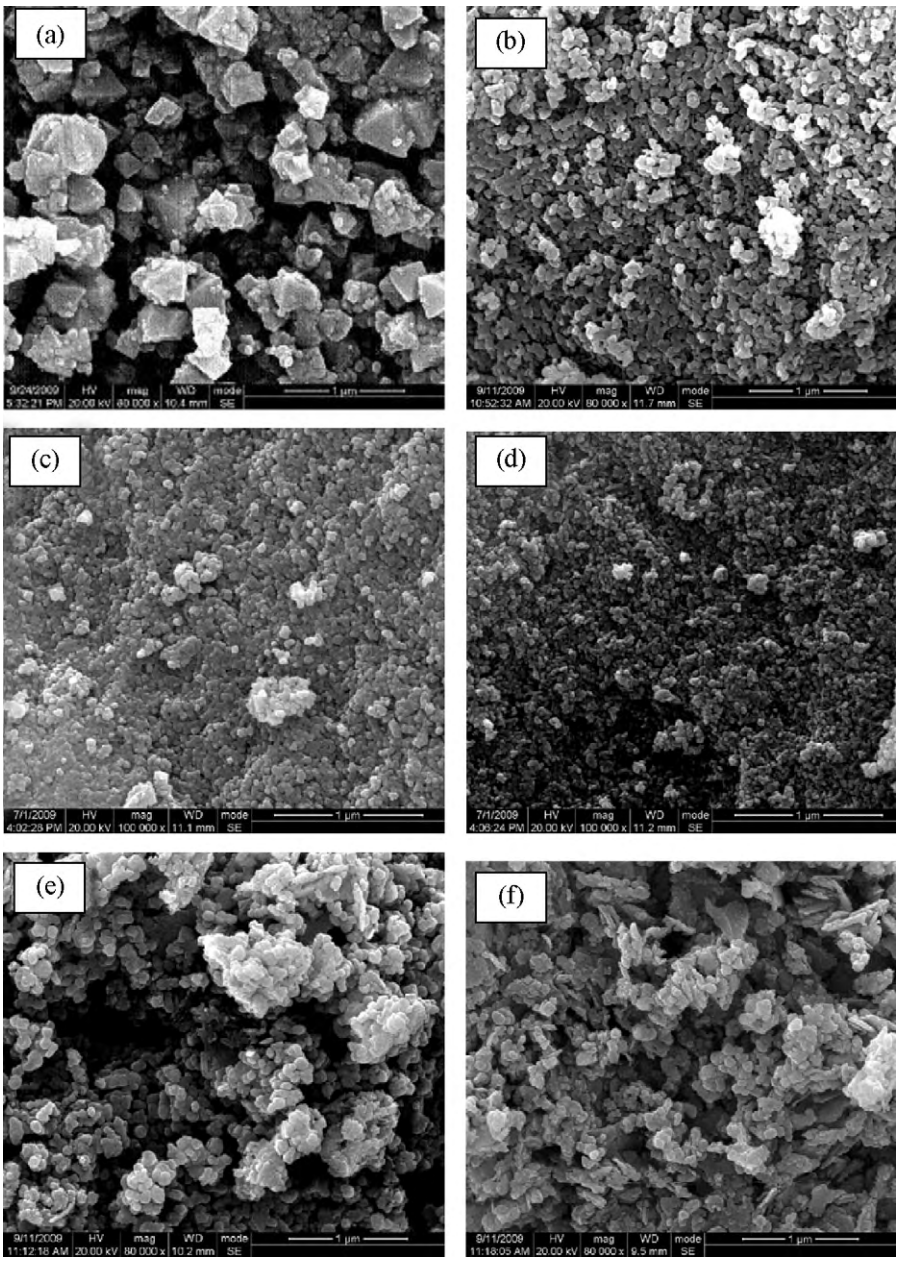

Fig. 3. SEM images of Fe_2O_3 prepared by different methods: (a) Fe_2O_3-L; (b) Fe_2O_3-UP; (c) Fe_2O_3-SG; (d) Fe_2O_3-ME; (e) Fe_2O_3-SS; (f) Fe_2O_3-MS.

with the reported binding energy of $2p_{3/2}$ for α-Fe_2O_3 [28]. For the other Fe_2O_3 samples, the binding energies are slightly lower due to the formation of γ-Fe_2O_3 during the preparation processes. The XRD studies also reveal the co-existence of α-Fe_2O_3 and γ-Fe_2O_3 in the other samples except for Fe_2O_3-L and Fe_2O_3-UP.

Fig. 4B illustrates the O 1s XPS spectra of the samples. It is observed that the O 1s region can be deconvoluted into two peaks at about 529.8 and 531.5 eV, which indicates the existence of two different oxygen species. It has been revealed that O_I with the lower B.E. at ~529.8 eV is characteristic of the "O^{2-}" ions of the lattice oxy-

Table 2
XPS characteristics of Fe 2p of Fe_2O_3 prepared by different methods.

Method	Binding energy (eV)			Fe $2p_{3/2}$–Fe $2p_{3/2}$,sat. mmmmb (eV)	Fe $2p_{3/2}$–Fe $2p_{1/2}$ (eV)
	Fe $2p_{3/2}$	Fe $2p_{3/2}$,sat.	Fe $2p_{1/2}$		
L	711.5 (4.0)[a]	718.3 (6.6)	725.4 (5.9)	7.8	13.9
UP	711.3 (4.0)	718.8 (6.3)	725.1 (6.1)	7.2	13.5
SG	711.1 (3.8)	718.9 (5.8)	724.7 (5.5)	7.8	13.6
ME	710.7 (3.5)	718.6 (6.4)	724.3 (5.3)	7.9	13.6
SS	710.8 (3.6)	718.8 (6.7)	724.4 (6.1)	8.0	13.6
MS	710.6 (3.7)	718.7 (6.9)	724.6 (5.7)	8.1	13.7

[a] Values in parentheses refer to FWHM in eV.

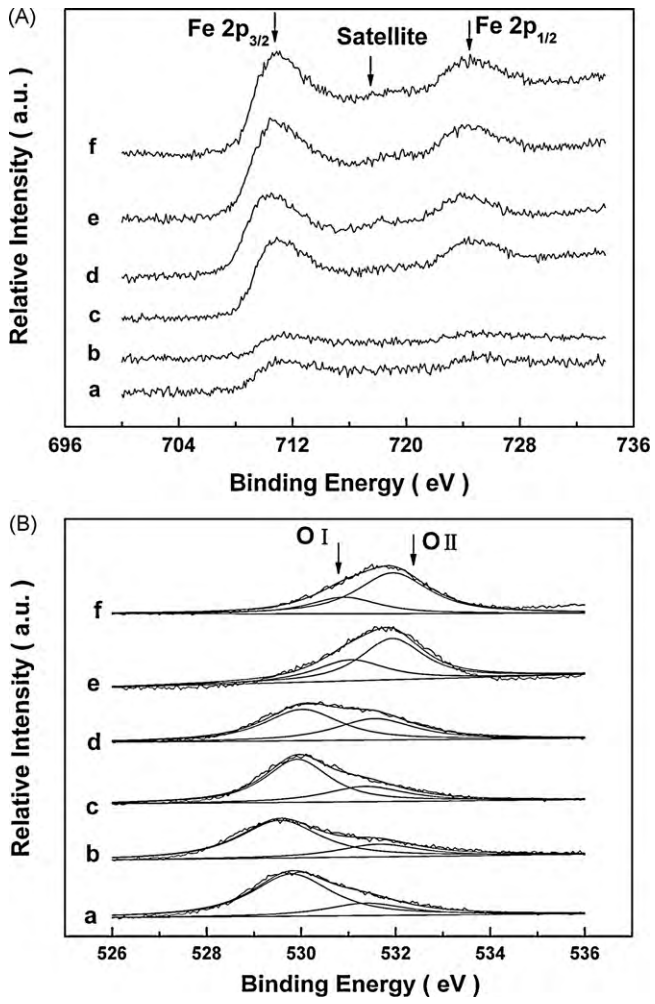

Fig. 4. XPS spectra of (A) Fe 2p and (B) O 1s of Fe_2O_3 prepared by different methods: (a) Fe_2O_3-L; (b) Fe_2O_3-UP; (c) Fe_2O_3-SG; (d) Fe_2O_3-ME; (e) Fe_2O_3-SS; (f) Fe_2O_3-MS.

gen, while O_{II} with the higher B.E. at ~531.5 eV is assigned to surface oxygen with lower electron density, described as surface oxygen species "O^-" [33,34]. The percentage of two surface oxygen species is summarized in Table 3. Note that the proportion of O_{II} shows a steady increase for Fe_2O_3-SS and Fe_2O_3-MS, which is probably relative to the increase of γ-Fe_2O_3 formed by the SS and MS methods, which is proved by the XRD results. This demonstrates that preparation method influences the crystal distribution of Fe_2O_3 as well as the percentage of oxygen species on the sample surface.

Table 3
XPS characteristics of O 1s of Fe_2O_3 prepared by different methods.

Method	Binding energy (eV)		Peak intensity[b] (%)	
	O_I	O_{II}	$I(O_I)$	$I(O_{II})$
L	529.8 (2.0)[a]	531.4 (2.0)	77.02	22.98
UP	529.6 (2.0)	531.7 (2.0)	74.78	25.22
SG	529.9 (1.6)	531.4 (2.0)	69.37	30.63
ME	530.0 (1.9)	531.6 (2.0)	58.06	41.94
SS	531.0 (1.8)	531.9 (1.6)	36.28	63.72
MS	530.9 (1.7)	531.9 (1.8)	28.80	71.20

[a] Values in parentheses refer to FWHM in eV.
[b] Intensity of the peaks in percentage of the total O 1s area.

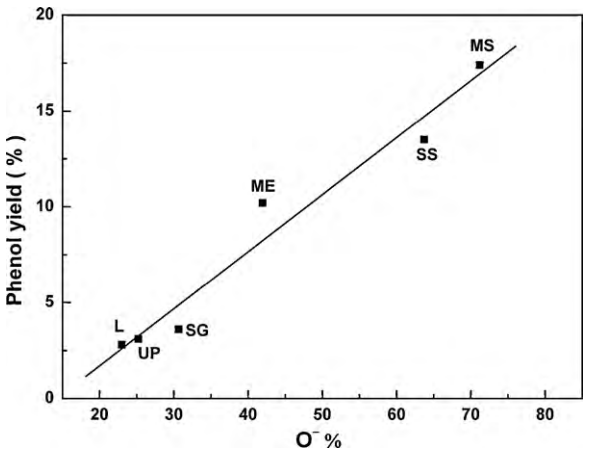

Fig. 5. The catalytic activities of Fe_2O_3 as a function of the content of O^-.

3.5. Catalytic activity

Fe_2O_3 prepared by different methods was used as catalyst for the hydroxylation of benzene to phenol with H_2O_2 as oxidant. Fig. 5 summarizes the correlation between the catalytic activity and the content of surface oxygen species "O^-". The single linear relationship is clearly confirmed. The higher activities are achieved with the SS and MS methods, especially at lower calcination temperature. It is obvious that the enhanced surface oxygen species "O^-" leads to better hydroxylation of benzene to phenol. It demonstrates that surface oxygen species "O^-" is the main factor of catalytic activity. The results suggest that surface oxygen species "O^-", which have higher mobility than lattice oxygen, can actively take part in some oxidation process and greatly contribute to the catalytic activity.

In addition, the control experiment without oxidant (H_2O_2) was conducted under the same conditions and no phenol was obtained, showing that Fe_2O_3 was not an oxidant. Over catalyst Fe_2O_3 prepared by thermal decomposition and ultrasonic-precipitation method, 2.8% and 3.1% of phenol yield is obtained. With the increase of the content of γ-Fe_2O_3, the phenol yield increases. 17.4% of phenol yield achieves with Fe_2O_3-MS catalyst, enhanced by 3.9 times with respect to Fe_2O_3 catalyst prepared by Zhang [24]. Therefore it can be concluded from this series of experiments that Fe_2O_3 acts actually as catalyst. Especially, γ-Fe_2O_3 is more active than α-Fe_2O_3 and bulk Fe_2O_3 for the hydroxylation of benzene to phenol under the conditions investigated in the present work. Misono [35] had found that the catalytic activity for oxidative dehydrogenation of butane was much higher with γ-Fe_2O_3 than with α-Fe_2O_3. Shrigadi [36] had found the same activity pattern in the Friedel-Crafts benzylation reaction. In fact, the same activity pattern for Fe_2O_3 catalyst for the hydroxylation of benzene to phenol is observed. The differences in their activity of α-Fe_2O_3 and γ-Fe_2O_3 could be attributed to the lattice structures [37]. γ-Fe_2O_3 and α-Fe_2O_3 have different lattice structures: ccp and hcp.

4. Conclusions

Nanosized Fe_2O_3 with similar morphology and approximately uniform particle size was prepared by five methods, and used for the hydroxylation of benzene to phenol. Preparation method significantly influences the crystal structure and distribution of γ-Fe_2O_3 and α-Fe_2O_3. Surface oxygen species "O^-" is the main factor of catalytic activity. γ-Fe_2O_3 is more active than α-Fe_2O_3 and bulk Fe_2O_3 for the hydroxylation of benzene to phenol under mild conditions. The differences in their activity of α-Fe_2O_3 and γ-Fe_2O_3 could be attributed to the lattice structures.

Acknowledgements

The financial support from the National Natural Science Foundation of China (no. 20872102), PCS IRT (no. 0846), determination for properties of catalysts from SEM, XRD, FT-IR Groups of Analytical and Testing Center of Sichuan University and from XPS Groups of Analytical and Testing Center of Chengdu Organic Chemicals Ltd. of Chinese Academy of Sciences, are greatly appreciated.

References

[1] J.H. Adair, T. Li, T. Kido, K. Havey, J. Moon, et al., Mater. Sci. Eng. R: Rep. 23 (1998) 139–342.
[2] A.J. Maira, K.L. Yeung, C.Y. Lee, P.L. Yue, C.K. Chan, J. Catal. 192 (2000) 185–196.
[3] S. Yatsuya, Y. Tsukasaki, K. Mihama, R. Uyeda, J. Cryst. Growth 45 (1978) 490–494.
[4] M. Catauro, C. Pagliuca, L. Lisi, G. Ruoppolo, Thermochim. Acta 381 (2002) 65–72.
[5] M. Yoshio, Y. Todorov, K. Yamato, H. Noguchi, et al., J. Power Sources 74 (1) (1998) 46–53.
[6] J.W. Geus, Appl. Catal. 15 (1986) 313–333.
[7] T. Fujii, M. Takano, R. Katano, Y. Bando, Y. Isozumi, J. Appl. Phys. 66 (1989) 3168–3172.
[8] O.K. Tan, W. Zhu, Q. Yan, L.B. Kong, Sens. Actuat. B: Chem. 65 (2000) 361–365.
[9] Y.J. Xiong, Z.Q. Li, X.X. Li, B. Hu, Y. Xie, Inorg. Chem. 43 (2004) 6540–6542.
[10] L.C. Varanda, M. Jafelicci Jr., G.F. Goya, J. Magn. Magn. Mater. 226 (2001) 1933–1935.
[11] H. Imai, M. Senna, J. Appl. Phys. 49 (1978) 4433–4437.
[12] D.M. Lind, S.D. Berry, G. Chern, H. Mathias, L.R. Testardi, Phys. Rev. B 45 (1992) 1838–1850.
[13] T.G. Carreño, A. Mifsud, C.J. Serna, J.M. Palacios, Mater. Chem. Phys. 27 (1991) 287–296.
[14] Y.S. Kang, S. Risbud, J.F. Rabolt, P. Stroeve, Chem. Mater. 8 (1996) 2209–2211.
[15] B. Gržeta, M. Ristić, I. Nowik, S. Musić, J. Alloys Compd. 334 (2002) 304–312.
[16] H. Orita, N. Itoh, Appl. Catal. A: Gen. 258 (2004) 17–23.
[17] X.B. Ke, L. Xu, C.F. Zeng, L.X. Zhang, N.P. Xu, Micropor. Mesopor. Mater. 106 (2007) 68–75.
[18] K.M. Parida, D. Rath, Appl. Catal. A: Gen. 321 (2007) 101–108.
[19] K. Lemke, H. Ehrich, U. Lohse, H. Berndt, K. Jähnisch, Appl. Catal. A: Gen. 243 (2003) 41–51.
[20] B.K. Paul, S.P. Moulik, J. Dispers. Sci. Technol. 18 (1997) 301–367.
[21] Y.S. Wang, A. Muramatsu, T. Sugimoto, Colloids Surf. A 134 (1998) 281–297.
[22] C. Walling, R.A. Johnson, J. Am. Chem. Soc. 97 (1975) 363–367.
[23] J.S. Choi, T.H. Kim, K.Y. Choo, J.S. Sung, M.B. Saidutta, S.O. Ryu, S.D. Song, B. Ramachandra, Y.W. Rhee, Appl. Catal. A: Gen. 290 (2005) 1–8.
[24] X.F. Zhang, J.C. Zhang, T.Q. Zhang, Sci. Technol. Chem. Ind. Chin. 9 (2001) 27–30.
[25] Y.K. Zhong, G.Y. Li, L.F. Zhu, Y. Yan, G. Wu, C.W. Hu, J. Mol. Catal. A: Chem. 272 (2007) 169–173.
[26] R.D. Waldron, Phys. Rev. 99 (1955) 1727–1735.
[27] W.B. White, B.A. DeAngelis, Spectrochim. Acta A 23 (1967) 985–995.
[28] V. Chhabra, P. Ayyub, S. Chattopadhyay, A.N. Maitra, Mater. Lett. 26 (1996) 21–26.
[29] T. González Carreño, A. Mifsud, C.J. Serna, J.M. Palacios, Mater. Chem. Phys. 27 (1991) 287–296.
[30] T. Fujii, F.M.F. de Grood, G.A. Sawatzky, F.C. Voogt, T. Hibma, K. Okada, Phys. Rev. B 59 (1999) 3195–3202.
[31] S. Bera, A.A.M. Prince, S. Velmurugan, P.S. Raghavan, et al., J. Mater. Sci. 36 (2001) 5379–5384.
[32] I. Banerjee, Y.B. Khollam, C. Balasubramanian, R. Pasricha, Scr. Mater. 54 (2006) 1235–1240.
[33] C. Yoon, D.L. Cocke, J. Catal. 113 (1988) 267–280.
[34] M. Muhler, R. Schlögl, G. Ertl, J. Catal. 138 (1992) 413–444.
[35] X.L. Tang, H.W. Zhang, H. Su, Z.Y. Zhong, Y.L. Jing, J. Solid State Chem. 179 (2006) 1618–1622.
[36] M. Misono, K. Sakata, F. Ueda, Y. Nozawa, Y. Yoneda, Bull. Chem. Soc. Jpn. 53 (1980) 648–652.
[37] N.B. Shrigadi, A.B. Shinde, S.D. Samant, Appl. Catal. A: Gen. 252 (2003) 23–35.